PROCESSES

Optimization of the cooling strategy during cryogenic milling of Ti-6Al-4 V when applying a sub-zero metalworking fluid

Kevin Gutzeit[1] · Maximilian Berndt[1] · Jonas Schulz[2] · Daniel Müller[1] · Benjamin Kirsch[1] · Erik von Harbou[2] · Jan C. Aurich[1]

Abstract

Due to an excellent ratio of high strength to low density, as well as a strong corrosion resistance, the titanium alloy Ti-6Al-4 V is widely used in industrial applications. However, Ti-6Al-4 V is also a difficult-to-cut material because of its low thermal conductivity and high chemical reactivity, especially at elevated temperatures. As a result, machining Ti-6Al-4 V is characterized by high thermal loads and a rapidly progressing thermo-chemical induced tool wear. An adequate cooling strategy is essential to reduce the thermal load and therefore tool wear. Sub-zero metalworking fluids (MWF) which are applied at liquid state but at supply temperatures below the ambient temperature, offer great potential to significantly reduce the thermal load when machining Ti-6Al-4 V. Within the presented research, systematically varied sub-zero cooling strategies are applied when milling Ti-6Al-4 V. The influences of the supply temperature, as well as the volume flow and the outlet velocity are investigated aiming at a reduction of the thermal loads that occur during milling. The milling experiments were recorded using high-speed cameras in order to characterize the impact of the cooling strategies and resolve the behavior of the MWF. Additionally, the novel sub-zero cooling approach is compared to a cryogenic CO_2 cooling strategy. The results show that the optimized sub-zero cooling strategy led to a sufficient reduction of the thermal loads and does outperform the cryogenic cooling even at elevated CO_2 mass flows.

Keywords Milling · Cooling strategy · Sub-zero MWF · Ti-6Al-4V · High-speed imaging

List of symbols

A	Cross section	$\dot{m}$	Mass flow
a_e	Width of cut	n	Rotational speed
a_p	Depth of cut	p	Supply pressure
c	Outlet velocity	RMS	Root mean square
c_p	Specific heat capacity	r_β	Cutting edge radius
D	Tool diameter	s	Seconds
d	Nozzle outlet diameter	T_{Max}	Maximum temperature
F	Force	T_{supply}	Supply temperature
Fps	Frames per second	v_c	Cutting speed
f_z	Feed per tooth	v_f	Feed velocity
l	Length	$\dot{V}$	Volume flow
		z	Number of teeth
		γ	Surface tension
		λ	Thermal conductivity
		ν	Viscosity
		ζ	Mass ratio
		ρ	Density

✉ Kevin Gutzeit
kevin.gutzeit@mv.uni-kl.de

[1] Institute for Manufacturing Technology and Production Systems, RPTU Kaiserslautern, Gottlieb-Daimler-Str., 67663 Kaiserslautern, Germany

[2] Laboratory of Reaction and Fluid Processing Engineering, RPTU Kaiserslautern, Gottlieb-Daimler-Str., 67663 Kaiserslautern, Germany

1 Introduction and state of the art

Titanium alloys, such as Ti-6Al-4 V, are widely used in industrial applications, due to a strong corrosion resistance as well as an excellent ratio of low density to high strength even at elevated temperatures [1, 2]. To achieve a favorable application behavior, mechanically and thermally highly stressed components are therefore made of Ti-6Al-4 V [3]. Despite these favorable characteristics, Ti-6Al-4 V has a very low thermal conductivity and a low heat capacity, leading to difficulties in heat dissipation during cutting [4]. Due to a limited heat transfer via the chips and the workpiece [5, 6], high cutting temperatures and thus high thermal loads occur in the cutting zone [7]. In addition, the titanium alloy Ti-6Al-4 V is characterized by a very high chemical reactivity, especially at higher temperatures, resulting in adhesive and chemical reactions between the tool and the workpiece [8]. Due to the high thermal loads and the chemical reactivity, a rapidly progressing tool wear is enhanced, reducing tool life and thus productivity [9]. Therefore, Ti-6Al-4 V is classified as a difficult-to-cut material [10].

To reduce the thermal load, metalworking fluids (MWF) are usually applied when cutting Ti-6Al-4 V. The performance of an MWF is driven by a complex combination of physical and chemical effects (e.g. capillary flow, Marangoni effect) [11]. The cooling effect is the result of the convective heat transfer. This heat transfer depends on the temperature gradient between the MWF, the tool and workpiece, as well as on the heat transfer coefficient [12].

An alternative to conventional MWF is the use of cryogenic cooling strategies. Carbon dioxide snow (CO_2) is one of the most commonly used cryogenic coolants [13]. The high cooling effect is achieved due to the low coolant temperatures of the CO_2 (-78.5 °C [14]). As a result, cryogenic cooling strategies can reduce tool wear and therefore increase the tool life in comparison to dry milling [15] or wet milling using a conventional MWF [16]. In addition to the low coolant temperatures, a favorable heat coefficient is desirable for a sufficient cooling effect. When applying CO_2 as a cryogenic coolant, the heat transfer is mainly achieved by a convection of gaseous CO_2 and the sublimation of solid CO_2 particles [17]. The use of a media supplied at liquid state often results in a comparatively higher heat transfer coefficient as well as better lubrication effects [18].

In previous works, sub-zero MWF were examined, that are applied at liquid state and at temperatures well below 0 °C, therefore combining the benefits of cryogenic and conventional flood cooling approaches [19]. Using a mixture of water and polyhydric alcohols as sub-zero MWF enables supply temperatures as low as –50 °C [20, 21].

As a result, a high heat transfer coefficient and therefore high cooling effects are favored during cutting. When turning Ti-6Al-4 V while using a sub-zero MWF, a favorable thermo-mechanical load was observed, resulting from the enhanced heat transfer in superposition with an improved lubrication. Consequently, a better surface quality and less tool wear was observed in comparison to cryogenic cooling approaches [21, 22]. First studies in sub-zero milling have also shown the potential for better surface integrity, less adhesion at the cutting edges as well as longer tool life compared to dry machining or the use of cryogenic cooling approaches [21, 22]. A systematic configuration of the sub-zero MWF application in terms of supply temperature, flow rate and nozzle outlet velocity was not yet conducted for milling, although it offers a high potential for increasing the efficiency of this novel cooling strategy.

In this work, the sub-zero cooling is varied in terms of supply temperature, volume flow and nozzle outlet velocity when milling. In addition to force and temperature measurements, high-speed recordings are also carried out in order to resolve the interactions of the MWF and the cutting process at varied states. For this purpose an image-based test setup including a high-speed camera and an illumination unit are integrated into the machining center. The focus of this study is the characterization of the interactions resulting from the temperature-dependent viscosity, the outlet velocity and the volume flow on the wetting and cooling effect of the sub-zero MWF.

2 Experimental setup

2.1 Characterization of the sub-zero MWF

A mixture of water and ethane-1,2-diol (MEG) was used as sub-zero MWF. Adding MEG to water causes a freezing point depression, therefore the mixture remains in a stable liquid state down to a temperature of -50 °C. The mixing ratio of water and MEG influences the thermal conductivity λ, the specific heat capacity c_p and the kinematic viscosity ν. Considering the heat transfer between the sub-zero MWF and the cutting zone, a low kinematic viscosity and a high heat capacity, as well as a high thermal conductivity are favorable [12, 23]. At 20 °C, Water ($\lambda = 0.55$ W/mK; $c_p = 4.2$ J/gK) inhibits a much higher thermal conductivity and specific heat capacity than MEG ($\lambda = 0.29$ W/mK, $c_p = 2.3$ J/gK) [12]. Furthermore, the viscosity of water ($\nu = 1$mm^2/s) is much lower than the viscosity of MEG ($\nu = 27$mm^2/s) [12], which is why a high amount of water is desirable.

Despite that, the surface tension of water ($\gamma = 72$mN/m) is higher than the surface tension of pure MEG ($\gamma = 47$mN/m) resulting in a less pronounced wetting capability [24, 25].
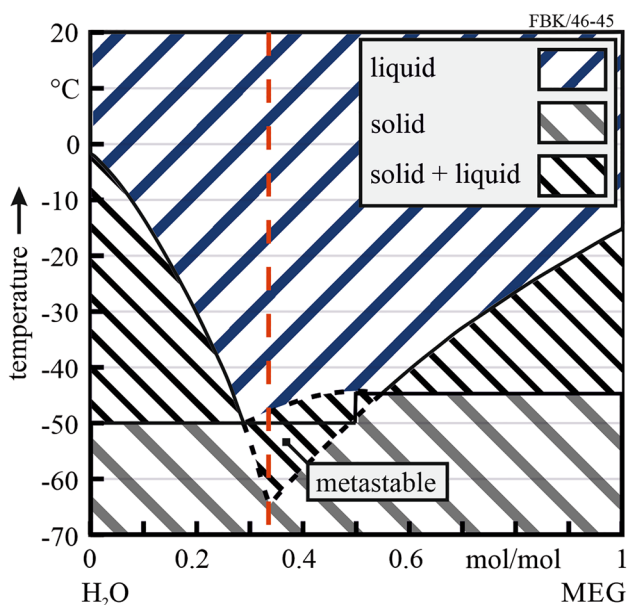
Fig. 1 Phase diagram of the sub-zero MWF mixture containing water and ethane-1,2 diol adapted from [12, 19, 27]
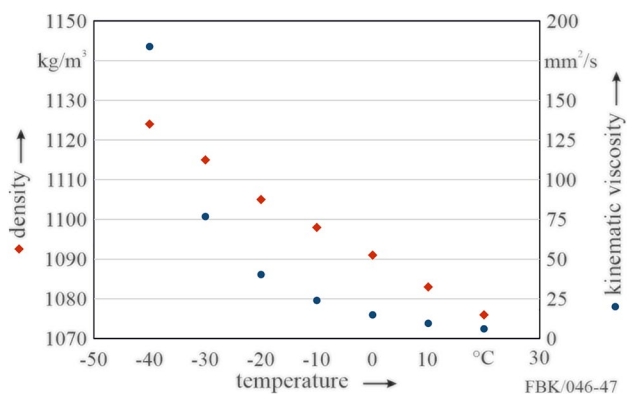

Fig. 2 Density and kinematic viscosity of the sub-zero MWF used as a function of its temperature

Thus, a higher amount of MEG is favorable regarding the wetting capability which improves the convective heat transfer [25, 26]. The used mixture is highlighted in the phase diagram in Fig. 1 corresponding to a mass ration of $\zeta_{MEG,Water} = 1.72$.

Besides the mixing ratio of the sub-zero MWF, the supply temperature does also influence the fluid properties. The viscosity is highly temperature dependent, as depicted in Fig. 2. Due to an increasing viscosity, the Reynolds number decreases strongly, therefore lowering the heat transfer. Furthermore, there are pressure losses in the supply system, due to an increased viscosity, which leads to a higher power consumption of the pump [24].

The sub-zero MWF performance is furthermore impacted by the additives within the coolant. In the sub-zero MWF used, disodium metasilicate (Na_2SiO_3) was added as a corrosion inhibitor with a concentration of 3.7 g per 1 kg sub-zero MWF. By adding disodium metasilicate to the sub-zero MWF, the wetting capability is also improved [28]. Additionally, 14 g acid tri-isobutyl ($C_{12}H_{27}O_4P$) was added per 1 kg of sub-zero MWF as an anti-wear agent. Hence, an improved MWF performance is achievable through advantageous fluid and flow properties, a good wetting ability as well as a high temperature gradient between the MWF and the cutting zone.

2.2 Machining experiments

Ti-6Al-4 V workpieces with a length of 100 mm and a cross-section of $A = 10 \times 10mm^2$ were machined via end milling. The experiments were carried out on a 5-axis machining center (Deckel Maho Gildemeister DMU 70 eVolution[1]). The experimental setup, as well as the tool and the cutting parameters used for all tests conducted are given in Fig. 3a.

In order to supply the sub-zero MWF to the cutting zone during milling operations, a new cooling system was developed and integrated into the machining center which
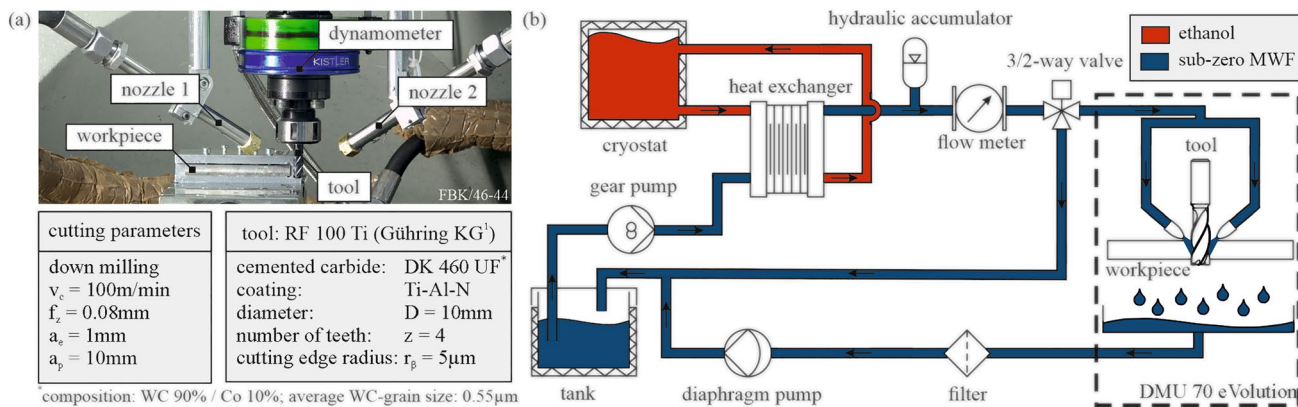

Fig. 3 Depiction and specification of the experimental setup (**a**) and schematic view of the sub-zero cooling system (**b**)

is schematically depicted in Fig. 3b. A gear pump (Verder M4X66EE8000TB-8[1]) is used to transport the sub-zero MWF at a maximum flow rate of 8 l/min which is suitable for milling operations. The combination of the cryostat (Huber Unistat630[1]) with a plate heat exchanger (Hydac HEX S522-40–00[1]) enables a stationary process with supply temperatures as low as –40 °C. Furthermore, a flexible adaption of the supply temperature during the milling process is possible. The 3/2-way valve is coupled with the NC control of the machining center to promote a controlled application of the coolant during the cutting tests. All components are thermally insulated to counteract thermal bridges and optimize the cooling performance.

Within this study, the influence of systematically varied cooling strategies on the thermo-mechanical load is examined during sub-zero end milling. A detailed specification of the investigated cooling strategies is depicted in Table 1. The supply temperature T_{supply}, the density ρ of the sub-zero MWF and the volume flow $\dot{V}$ were measured using a Coriolis flow meter (Siemens FCS 400[1]). The resulting mass flow $\dot{m}$, the outlet velocity c and the supply pressure p were calculated according to Eq. 1 – Eq. 3. In a first step, the influence of a decreasing supply temperature is investigated at a constant volume flow. Since the volume flow was kept constant, the mass flow increases at lower supply temperatures due to the increasing density of the MWF (Fig. 2). Then, the influence of the volume flow is characterized at a constant supply temperature. Here, two different rouse nozzle outlet diameters of d = 1 mm and d = 2 mm were used. This was done in order to investigate the influence of the outlet velocity as well as the supply pressure of the sub-zero MWF at constant volume flows.

$$\dot{m} = \dot{V}\rho \tag{1}$$

$$c = \dot{V}\big/\left[2 * \pi * (d/2)^2\right] \tag{2}$$

$$\Delta p = \rho\, c^2\big/2 \tag{3}$$

For reference, additional milling experiments based on cryogenic cooling with CO_2 were carried out. Here, the mass flow of the CO_2 was systematically varied by utilizing different nozzle outlet diameters (Table 2). The cryogenic coolant was stored in a siphoned gas cylinder at ambient temperature. The CO_2 was supplied to the cutting zone with an outlet temperature of –78.5 °C [14]. Before starting each test, a uniform workpiece temperature of 20 °C was ensured. Three tests were carried out for every cooling strategy investigated.

2.3 Measurement technology

During cutting, the occurring force components F_x, F_y and F_z were measured using a rotating dynamometer

Table 2 Specification of the cryogenic CO_2- cooling strategies:

Supply temperature in °C	Mass flow in kg/min	Outlet diameter in mm
− 78.5	0	0
− 78.5	0.2	0.25
− 78.5	0.7	0.50
− 78.5	1.5	0.75
− 78.5	2.7	1.00

Table 1 Specification of the cooling strategies investigated when using the sub-zero MWF

Supply temperature in °C	Volume flow in l/min	Mass flow in kg/min	Outlet diameter in mm	Outlet velocity in m/s	Supply pressure in bar
20	3.60	3.87	2	9.55	0.49
0	3.60	3.93	2	9.55	0.50
− 10	3.60	3.95	2	9.55	0.50
− 20	3.60	3.98	2	9.55	0.50
− 30	3.60	4.01	2	9.55	0.51
− 40	3.60	4.05	2	9.55	0.51
− 30	1.80	2.01	2	4.77	0.13
− 30	2.70	3.01	2	7.16	0.29
− 30	3.60	4.01	2	9.55	0.51
− 30	4.50	5.02	2	11.94	0.79
− 30	5.40	6.02	2	14.32	1.14
− 30	1,80	2.01	1	19,10	2.03
− 30	2.70	3.01	1	28.65	4.58
− 30	3.60	4.01	1	38.20	8.13

(Kistler Type 9123C[1]) with a sampling frequency of 15 kHz. The respective RMS was calculated to determine the resulting force via vector addition of the three force components.

Using a sampling frequency of 1 kHz and three K thermocouples (NiCr-Ni) with a diameter of 1 mm, the temperature was measured inside the workpiece. The distance between the tip of the thermocouple and the final machined surface was 0.3 mm. The thermocouples were positioned inside eroded holes ($\varnothing = 1.3$ mm) alongside the feed path with a respective distance of 15 mm to each other (see Fig. 4a). This results in a total of nine temperature measurements per case investigated. Before inserting each thermocouple, the holes were filled with thermal paste.

Representative temperature profiles are depicted in Fig. 4 for the three thermocouples used. For every temperature profile, a local minimum is observed since the cooling leads to a decreasing workpiece temperature. After the minimum temperature is reached, the temperature rises to a local maximum, as a result of the heat introduced during cutting. The maximum temperature results from the heat introduced by the tool, counteracting the heat removed by the coolant. Therefore, the maximum temperature is used to indicate the thermal load during milling while the minimum temperature is used to evaluate the cooling performance in dependence of the cooling strategy applied.
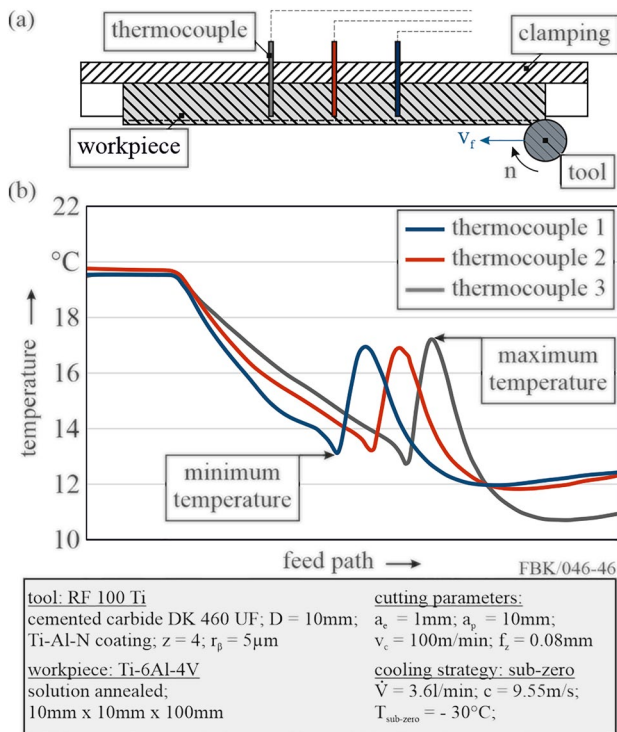
The milling process was recorded with a high-speed camera system (NX 8, Integrated Design Tools (IDT) Inc.[1]) in order to precisely resolve the wetting behavior of the sub-zero MWF on the tool and workpiece. An entocentric lens with a fixed focal length (atx-i 100 mm F2.8 FF Macro, Tokina Co. Ltd.[1]) enabled a perspectival shot of the test setup and by that a thorough imaging of the wetting phenomena. The illumination unit (miniConstellation™ 120, IDT Inc.[1]) was positioned with an offset of 50° to the high-speed camera. Metal housings with a 3'' inspection window (Mammut M/L IP65, autoVimation GmbH[1]) were used for the protection of the camera and the illumination unit from dust and hose water. A ball joint holder (Mounting Kit 16 m, autoVimation GmbH[1]) enabled a simple and flexible positioning of both housings. A constant flushing of the housings with pressurized air avoided overheating of the equipment. The experiments were recorded with an aperture setting of f/11 and an acquisition frame rate of 5350fps. The exposure time was set to 100 μs. The recordings were captured without gain enhancement and a manual acquisition start was sufficient for the examination of the wetting phenomena. Each experiment consisted of 500 frames and thereby showed a time period of 0.09 s. The test setup including the high-speed camera and illumination unit is depicted in Fig. 5.

3 Results and discussion

3.1 Cryogenic milling

In Fig. 6, the thermo-mechanical load is depicted in dependence of the mass flow during cryogenic milling with CO_2. Both the minimum and maximum temperature decrease at higher mass flows. As the cutting parameters and therefore

Fig. 4 Schematic view of the positioning of the thermocouples (**a**) and representative temperature profile measured inside the workpiece surface layer (**b**)
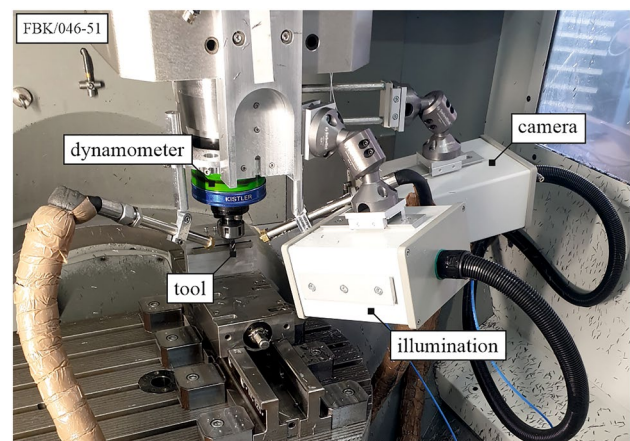

Fig. 5 Image-based test setup including high-speed camera and illumination unit

Fig. 6 Thermo-mechanical load in dependence of the mass flow during cryogenic milling
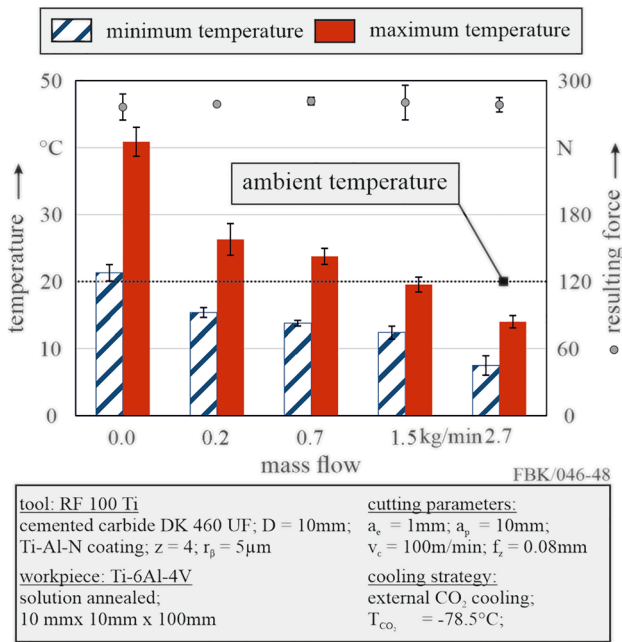

Fig. 7 Thermo-mechanical load in dependence of supply temperature during sub-zero milling

the duration of the milling process were kept constant, more CO_2 is applied at increased mass flows when milling. Consequently, the higher amount of cryogenic coolant is able to remove more heat from the cutting zone resulting in lower temperatures. In case of dry milling, the minimum temperature is close to the ambient temperature since no coolant is applied to remove the heat. As an average maximum temperature $T_{Max} = 41$ °C ± 2 °C was measured within the workpiece. In general, during dry milling of Ti-6Al-4 V, a much higher thermal load is expected in the cutting zone. The comparably low maximum temperatures measured here can be explained by the distance between the tip of the thermocouple and the actual cutting zone and the low thermal conductivity of the titanium alloy. As a result, comparably low temperatures were measured inside the workpiece, while the thermal loads directly in the cutting zone are expected to be much higher. However, since the process parameters were kept identical for all cooling strategies examined, the temperatures measured here can still be used to interpret the influence of the cooling strategies on the cooling performance and the occurring thermal loads.

With respect to the resulting forces that have occurred during cryogenic milling, no significant influence of the mass flow and the interlinked workpiece temperatures is observed (Fig. 6). This can be explained by the superposition of two opposing effects. A reduction of the temperature causes an increase in the material resistance, which results in increasing cutting forces. But decreasing temperatures also promote a shrinkage of the workpiece material, which
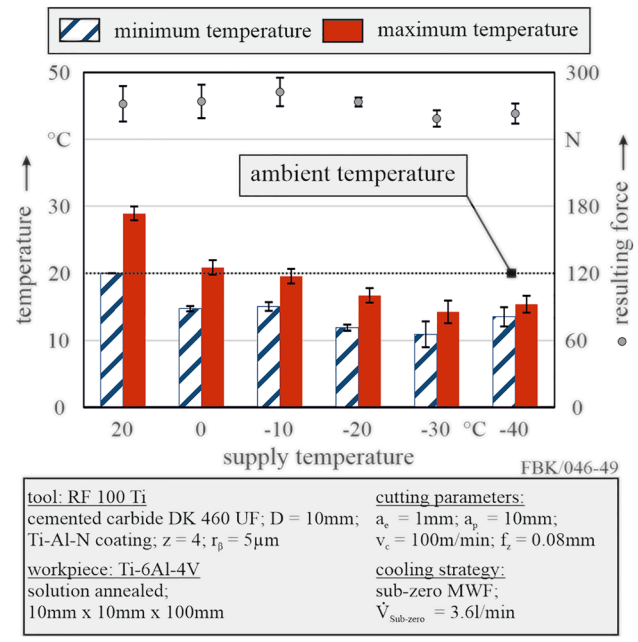
reduces the chip cross section and thus the forces that occur. These effects were also observed in previous studies by us [29].

3.2 Sub-zero milling

The occurring temperatures and forces during sub-zero milling are depicted in Fig. 7 in dependence of the supply temperature of the sub-zero MWF. While the volume flow and the outlet velocity were kept constant here, the mass flow and consequently the supply pressure slightly increase with decreasing supply temperatures (Table 1). The minimum temperature decreases when decreasing the supply temperature. This is expected as the increased temperature gradient increases also the heat flux from the surface of the workpiece to the MWF. However, when changing the supply temperature from $T_{supply} = -30$ °C to $T_{supply} = -40$ °C a slightly higher minimum temperature was measured. The effect of the supply temperature of the sub-zero MWF on its kinematic viscosity represents a potential reason for this phenomenon. As the kinematic viscosity increases exponentially with decreasing temperatures (Fig. 3) the highly viscous state of the MWF prevents a sufficient wetting, especially in the cutting zone. Consequently, less MWF reaches the cutting zone so that the heat transfer coefficient and the heat flux between surface of the workpiece and MWF is reduced.

This assumption is supported by the high-speed imaging depicted in Fig. 8. Here, the cutting process is depicted

Fig. 8 Images of the cutting process during sub-zero milling at supply temperatures of 20 °C (**a**), 0 °C (**b**) and –30 °C (**c**) at a constant mass flow and a nozzle diameter of d = 2 mm
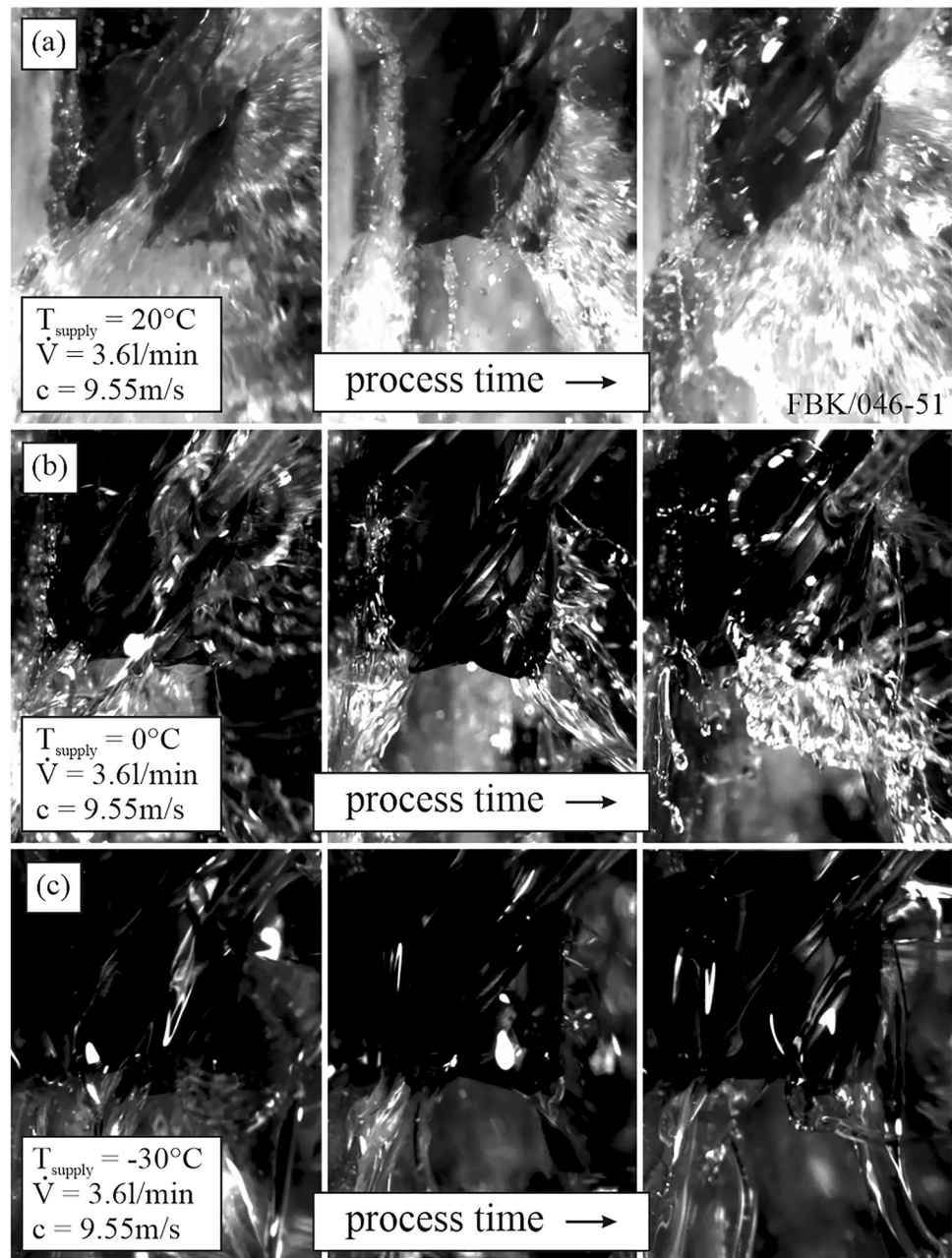
via three representative images in dependence of the supply temperature at a constant volume flow and outlet velocity. As the supply temperature decreases, the increasing viscosity of the MWF is clearly visible. A detailed depiction of the cutting process is given in the Online Resource 1.

A similar trend is observed for the maximum temperature. Since the process parameters and therefore the process kinematics were kept identical for all experiments, the heat introduced by the cutting process can be considered to be roughly identical. As a result, the change of the maximum temperature and by that the thermal load has to result from the different cooling performances characterized by the minimum temperature.

As with cryogenic machining, no significant effect of the cooling strategy on the resulting forces is observed. Despite that, the resulting forces are in general slightly lower during sub-zero milling which can be attributed to favourable lubrication effects.

In Fig. 9, the workpiece temperatures are depicted as a function of the volume flow during sub-zero milling at a constant supply temperature of $T_{supply} = -\,30$ °C. In general, a higher volume flow results in a promoted cooling performance and a decreasing thermal load since more coolant is applied to remove the heat from the cutting zone. Additionally, the outlet velocity and the supply pressure are increased when increasing the volume flow at a constant
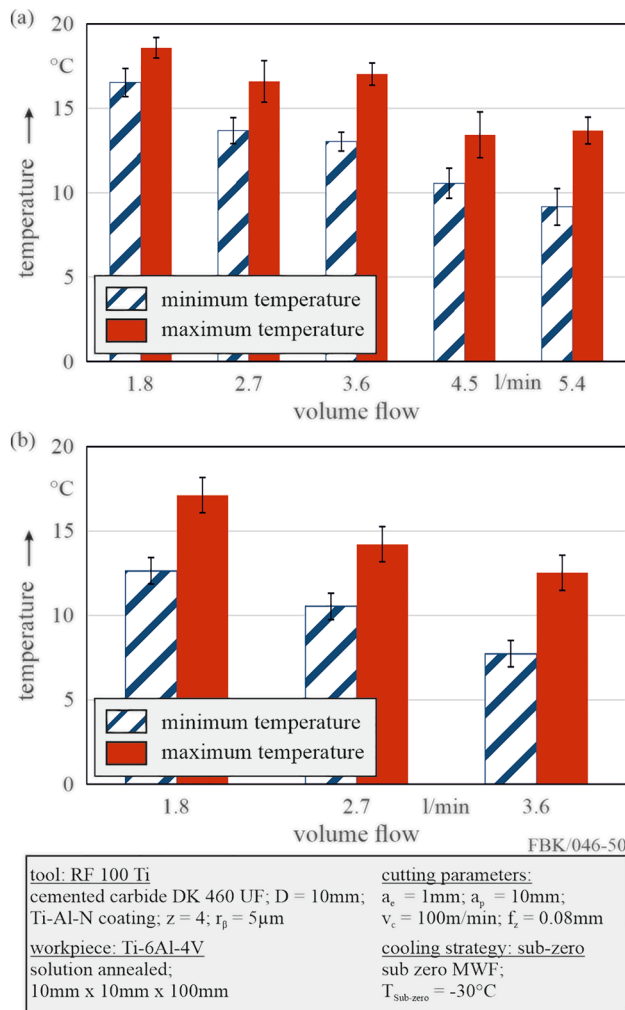
Fig. 9 Thermal load in dependence of the volume flow during sub-zero milling with a nozzle outlet diameter of 2 mm (**a**) and 1 mm (**b**)

process via three representative pictures. Here, the supply temperature and the resulting viscosity as well as the volume flow of the sub-zero MWF were kept constant. However due to the smaller nozzle outlet diameter (Fig. 10a) a thinner sub-zero MWF jet and a higher outlet velocity were realized. Due to the higher outlet velocity and the respectively higher outlet pressure, the promoted application behavior is clearly visible. A detailed depiction of the process is presented within the Online Resource 2.

As a result, the highest cooling performance and the lowest thermal load were measured when the highest outlet velocity was used at a moderate volume flow of $\dot{V} = 3.6$ l/min and a supply temperature of $T_{supply} = -30$ °C (Fig. 9b). Comparing this optimized sub-zero cooling strategy with the best performing referential cryogenic cooling strategy ($\dot{m} = 2.7$ kg/min, Fig. 6), a similar minimum temperature is observed despite the CO_2 having a much lower supply temperature. But due to the higher heat coefficient of the liquid sub-zero MWF, a comparable cooling performance is realized. With respect to the maximum temperatures of the two cooling strategies, sub-zero milling outperforms the cryogenic cooling as lower thermal loads were measured here. Despite having a similar cooling performance, the better lubrication effects of the sub-zero cooling can reduce the friction during cutting, therefore reducing the amount of heat being generated in the first place and the thermal load respectively. This becomes evident when comparing the differences between the minimum and maximum temperatures within this study. For sub-zero milling, these differences are much smaller, indicating a lower amount of heat being introduced by the cutting process. Due to identical process parameters across all tests, the reduced amount of heat can only be explained by the reduction of friction due to lubrication.

4 Summary

Within this study, a novel cooling system is presented to apply sub-zero MWF under various cooling strategies for milling operations. The presented setup allows a systematic adjustment of the supply temperature, the volume flow as well as the outlet velocity and the respective supply pressure. Aiming at an increased cooling performance and a reduced thermal load within the workpiece, the influences of these parameters were examined during end milling experiments.

The results show that the temperatures inside the workpiece decrease with decreasing supply temperatures of the MWF since the higher thermal gradient promotes the required cooling performance. Reducing the supply temperature also results in an exponential increase of the kinematic viscosity of the MWF. When the MWF exceeds a critical viscous state, a sufficient wetting of the cutting zone is

outlet diameter favoring an improved cooling. In order to characterize the impact of the volume flow, the outlet velocity, and the respective supply pressure, two different nozzle outlet diameters of d = 2 mm (Fig. 8a) and d = 1 mm (Fig. 8b) were examined.

At a constant volume flow, lower minimum and maximum temperatures are reached when using the smaller nozzle outlet diameter, since higher outlet velocities and supply pressures result here. The increase of the outlet velocity favors the convective heat transfer and therefore the cooling performance. Furthermore, a higher supply pressure promotes a better application of the sub-zero MWF into the cutting zone. Consequently, increasing the outlet velocity and the respective supply pressure by reducing the nozzle outlet diameter has a more favorable impact than increasing the volume flow.

In Fig. 10, the application of the sub-zero MWF with two different nozzle outlet diameters is shown during the cutting

Fig. 10 Images of the cutting process during sub-zero milling using a nozzle outlet diameter of 1 mm (**a**) and 2 mm (**b**)
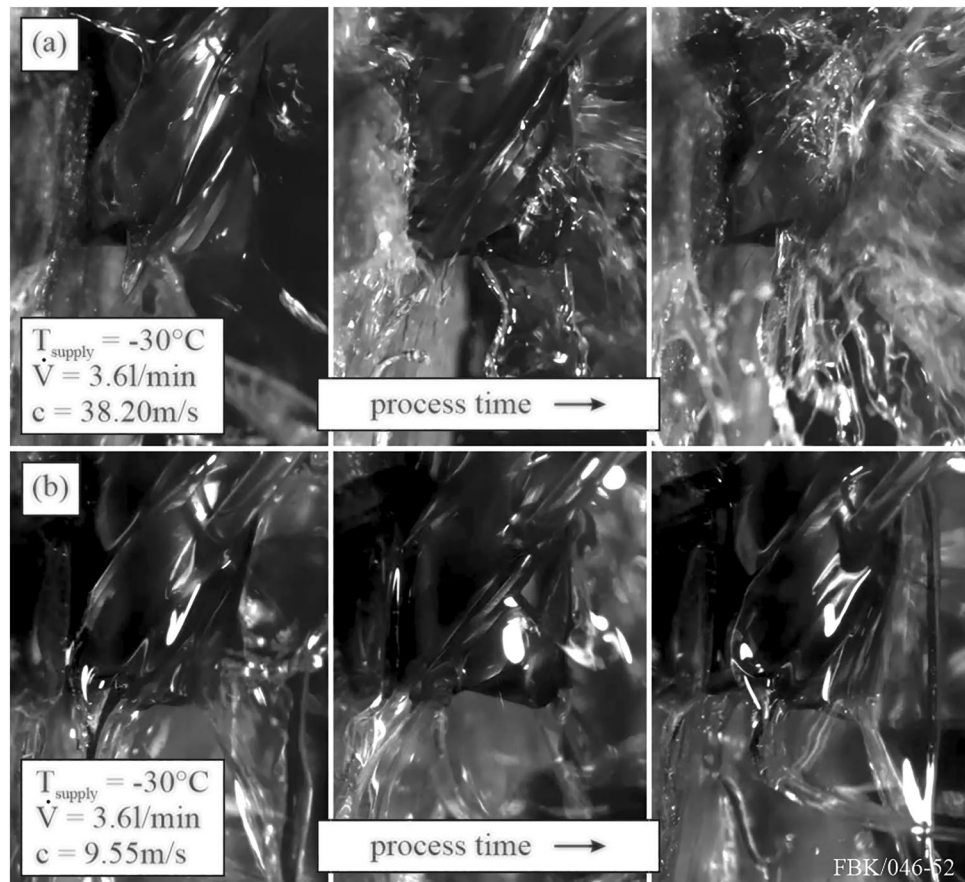
hindered resulting in higher temperatures in the workpiece. Within the frame of these experiments, an ideal supply temperature is found for $T_{supply} = -30$ °C.

Increasing the volume flow as well as the outlet velocity also leads to an improved cooling performance and hence to a reduction of the thermal loads. Here, the impact of the outlet velocity and the respective supply pressure is more significant in comparison to the volume flow, due to the beneficial influence regarding the conductive heat transfer and the promoted wetting of the cutting zone.

For reference, additional experiments were conducted using a cryogenic CO_2 cooling strategy with a supply temperature of $T_{supply} = -78.5$ °C and a systematical variation of the mass flow. Increasing the mass flow leads to an improved cooling performance as more cryogenic coolant is supplied to the cutting zone. However, despite the higher supply temperature, the optimized sub-zero cooling strategy outperforms the cryogenic cooling even at elevated CO_2 mass flows.

Future work will examine the application of the sub-zero MWF during milling operations in more detail. In particular, the influence of the cooling strategy on the thermo-mechanical load and the resulting surface integrity under variation of the cutting parameters will be analyzed. Furthermore, the performance of the developed sub-zero cooling strategy will be compared with conventional MWF in respect of the occurring loads as well as the resulting tool wear.

References

1. Peters M, Kumpfert J, Ward CH, Leyens C (2003) Titanium alloys for aerospace applications. Adv Eng Mater 5:419–427. https://doi.org/10.1002/adem.200310095

2. Inagaki I, Takechi T, Shirai Y, Ariyasu N (2014) Application and features of titanium for the aerospace industry. Nippon Steel Sumitomo Metal Tech Rep 106:22–27

3. Gonzalez H, Pereira O, Lopez de Lacalle LN, Calleka A, Ayesta I, Munoa J (2021) Flank-milling of integral blade rotors made in Ti6Al4V using cryo CO2 and minimum quantity lubrication (MQL). J Manuf Sci Eng 143:1–16. https://doi.org/10.1115/1.4050548

4. Ezugwu EO, Bonney J, Yamane Y (2003) An overview of the machinability of aeroengine alloys. J Mater Process Technol 134:233–253. https://doi.org/10.1016/S0924-0136(02)01042-7

5. Barry J, Byrne G, Lennon D (2001) Observations on chip formation and acoustic emission in machining Ti-6Al-4V alloy. Int J Mach Tools Manuf 41:1055–1070. https://doi.org/10.1016/S0890-6955(00)00096-1

6. Ginting A, Nouari M (2009) Surface integrity of dry machined titanium alloys. Int J Mach Tools Manuf 49:325–332. https://doi.org/10.1016/j.ijmachtools.2008.10.011

7. Ezugwu EO, Wang ZM (1997) Titanium alloy and their machinability – a review. J Mater Process Technol 68:262–274. https://doi.org/10.1016/S0924-0136(96)00030-1

8. Corduan N, Hirnbert T, Poulachon G, Dessoly M, Lambertina M, Vignneau J, Payoux B (2003) Wear mechanisms of new tool materials for Ti-6Al-4V high performance machining. CIRP Ann 52:73–76. https://doi.org/10.1016/S0007-8506(07)60534-4

9. Zoya ZA, Krishnamurthy R (2000) The performance of CBN tools in the machining of titanium alloys. J Mater Process Technol 100:80–86. https://doi.org/10.1016/S0924-0136(99)00464-1

10. Cotterell M, Byrne G (2008) Dynamics of chip formation during orthogonal cutting of titanium alloy Ti-6Al-4V. CIRP Ann Manuf Technol 57:93–96. https://doi.org/10.1016/j.cirp.2008.03.007

11. Brinksmeier E, Meyer D, Huesmann-Cordes AG, Herrmann C (2015) Metalworking fluids—mechanisms and performance. CIRP Ann Manuf Technol 64:605–628. https://doi.org/10.1016/j.cirp.2015.05.003

12. Stephan P, Kabelac S, Kind M, Mewes D, Schaber K, Wetzel T (2019) VDI heat Atlas, 12th edn. Springer

13. Jawahir LS, Attia H, Biermann D, Duflou J, Klocke F, Meyer D, Newmann ST, Pusavec F, Putz M, Rech J, Schulze V, Umbrello D (2016) Cryogenic manufacturing processes. CIRP Ann 65:13–36. https://doi.org/10.1016/j.cirp.2016.06.007

14. Barber CR (1997) The sublimation temperature of carbon dioxide. Br J Appl Phys 17:391–397

15. Gutzeit K, Basten S, Kirsch B, Aurich JC (2021) Verschleißuntersuchungen bei der kryogenen Zerspanung von Ti-6Al-4V. ZWF – Zeitschrift für wirtschaftlichen Fabrikbetrieb 116:452–455. https://doi.org/10.1515/zwf-2021-0121

16. Sadik MI, Isakson S, Malakizdai A, Nyborg L (2016) Influence of coolant flow rate on tool life and wear development in cryogenic and wet milling of Ti-6Al-4V. Proc CIRP 46:91–94. https://doi.org/10.1016/j.procir.2016.02.014

17. Zhan XR, Yamaguchi H (2011) An experimental study on heat transfer of CO2 solid-gas two phase flow with dry ice sublimation. Int J Therm Sci 50:2228–2234. https://doi.org/10.1016/j.ijthermalsci.2011.05.019

18. Basten S, Kirsch B, Merz R, Kopnarski M, Hasse H, Aurich JC (2020) Adsorption and reaction layers when turning AISI 304 using various cooling strategies. Procedia CIRP 87:125–130. https://doi.org/10.1016/j.procir.2020.02.100

19. Kirsch B, Basten S, Hasse H, Aurich JC (2018) Sub-zero cooling: a novel strategy for high performance cutting. CIRP Ann 67:95–98. https://doi.org/10.1007/978-3-030-03451-1_31

20. Basten S, Kirsch B, Gutzeit K, Hasse H, Aurich JC (2020) Influence of the supplying technique of a sub-zero metalworking fluid on the performance of face turning of Ti-6Al-4V titanium alloy. MIC Procedia 20:123–131. https://doi.org/10.1515/zwf-2021-0121

21. Gutzeit K, Müller D, Kirsch B, Aurich JC (2022) Influence of the cutting edge radius on tool wear during cryogenic machining with cemented carbide end mills. Proceedings of the 20th Plansee Seminar: International Conference on Refractory Metals and Hard Materials: 1–11.

22. Gutzeit K, Bulun G, Stelzer G, Kirsch B, Seewig J, Aurich JC (2022) Investigation of the surface integrity when cryogenic milling of Ti-6Al-4V using a sub-zero metalworking fluid. Proc CIRP 108– Proc 6th CIRP Conf Surf Integr 108:25–30. https://doi.org/10.1016/j.procir.2022.03.010

23. Basten S, Kirsch B, Hasse H, Aurich JC (2020) Formulation of sub-zero metalworking fluids for cutting processes: influence of additives. CIRP-JMST 31:25–33. https://doi.org/10.1016/j.cirpj.2020.09.006

24. Jasper JJ (1972) The surface tension of pure liquid compounds. J Phys Chem Ref Data 1:841–1010. https://doi.org/10.1063/1.3253106

25. Choi C, Kim M (2011) Wettability effects on heat transfer. In: Ahsan A (ed) Two phase flow, phase change and numerical modeling. InTech, pp 311–340

26. Moon JH, Cho M, Lee SH (2016) Dynamic wetting and heat transfer characteristics of a liquid droplet impinging on heated textured surfaces. Int J Heat Mass Transf 97:308–317. https://doi.org/10.1016/j.ijheatmasstransfer.2016.02.041

27. Ott JB, Goates JR, Lamb J (1972) Solid-liquid phase equilibria in water + ethylene glycol. J Chem Thermodyn 4:123–126. https://doi.org/10.1016/S0021-9614(72)80015-6

28. Steber J (2007) The ecotoxicity of cleaning product ingredients. In: Josef S (ed) Handbook for cleaning/decontamination of surfaces. Chapter 3 - the ecotoxicity of cleaning product ingredients. Elsevier, UK, pp 721–746

29. Gutzeit K, Hotz H, Kirsch B, Aurich JC (2020) Influence of nozzle position during cryogenic milling of Ti-6Al-4V. Production at the leading edge of technology - Proceedings of the 10th Congress of the German Academic Association for Production Technology (WGP), 284–293. https://doi.org/10.1007/978-3-662-62138-7_29